



# AN EXPERIMENTAL STUDY OF THE IMPULSE RESPONSE OF A VIBRO-IMPACTING CANTILEVER BEAM

D. J. WAGG\*, G. KARPODINIS AND S. R. BISHOP

Centre for Nonlinear Dynamics and its Applications, University College London, Gower Street, London WC1E 6BT, England

(Received 22 June 1998, and in final form 1 March 1999)

The dynamics of a vibro-impacting cantilever beam experiment using an impact load cell is considered. The signal recorded from the cell produces *spike train*-type data. The issues related to the analysis of such data are discussed; particularly the sampling rate and threshold values. For vibro-impact motion of the beam, the duration of impacts is investigated by using a time of contact measure. The implications are discussed for vibro-impact systems mathematically modelled by using instantaneous impact assumptions (coefficient of restitution). Using the load cell to measure impact forces for the beam system is also considered. Then a delay reconstruction of the dynamics of the system by using *interspike intervals* is considered. It is demonstrated how this process is effected by the influence of noise and the data-acquisition process using numerical simulations of the experimental data. It is shown how simple periodic motions can be identified by using a probability density approach and possible future research is highlighted.

© 1999 Academic Press

## 1. INTRODUCTION

The dynamics of a steel cantilever beam subject to harmonic forcing with a motion limiting constraint on one side is considered. For a range of values for the forcing frequency, impacts between the beam and the constraint can occur, resulting in vibro-impact motion of the beam. The dynamics of a vibro-impacting cantilever beam have been studied experimentally by several authors as an example of a simple non-linear dynamical system [1–4]. For systems which are linear away from the constraint, such as the beam system vibrating with small amplitude displacements, non-linearity in the system is induced by the non-smooth nature of the impact.

In the present study, attention is focussed on the dynamics of the beam via an experimentally recorded signal from the constraint (or impact stop). The aim is to interpret and predict dynamical behaviour by using this information alone. The experimental apparatus is the same as that used by Bishop *et al.* [4], with the

\*Current address: Earthquake Engineering Research Centre, University of Bristol, Queen's Building, University Walk, Bristol BS8 1TR, England

addition of a specially constructed *impact load cell* to measure the force imparted to the stop by the beam at each contact. The load cell was constructed by using strain gauges mounted on a thin-wall aluminium tube, such that the longitudinal displacement of the tube is measured (as strain) and then related to the force of impact. This technique has similarities with the sensing block method [5], for measuring an impact force by using strain gauges mounted on a “block”. Measurement of impact forces has important applications in the design of machine parts or structural components which are subject to impact loading.

Also of importance for design of engineering systems is the accurate mathematical modelling of the global dynamics of the system. Many of the theoretical and numerical studies of vibro-impact dynamics have been carried out by using an instantaneous impact rule [6–10]. This impact rule takes the form of a coefficient of restitution rule, where the coefficient is assumed to be a constant value related to the ratio of velocities before and after impact. Assuming that this change in velocity is instantaneous simplifies the analysis of the global dynamics of the system considerably, but in real systems the contact duration will always be of a finite duration. In reference [4] it was demonstrated that the use of such an impact law in a simple mathematical model could capture all the qualitative dynamics of the cantilever beam system. This was based on the premise that the time of contact was “short” compared to the time between impacts. Thus, a second purpose of this study was to quantify this assumption for the cantilever beam system, therefore giving an indication of possible use for this type of model for other similar engineering systems. In order to achieve this we define a *contact time measure* and consider typical values from the cantilever beam system.

The recorded experimental signal from the load cell consisted of a series of impulsive spikes, often referred to as *spike trains* [11, 12]. The issues associated with acquiring and processing this type of data such as sampling rate and spike identification by using threshold values are briefly considered. The analysis of spike data also has applications in the analysis of biomedical data [12]. These issues are significant when attempting to reconstruct the dynamics of a noisy (i.e., experimental) system by using *interspike intervals* [13]. The interspike interval technique is applied to the experimental data recorded from the cantilever beam system. Then it is explained how disturbance effects are introduced by the data-acquisition process and the subsequent limitations of the interspike interval approach.

## 2. EXPERIMENTAL APPARATUS

A schematic representation of the specially constructed impact load cell used for this study is shown in Figure 1. The aim was to design a load cell capable of detecting longitudinal impacts with forces as low as 1 N. In order to achieve this the strain gauges were mounted on a aluminum tube with a wall thickness of 0.23 mm. To detect a force of 1 N the gauges need to detect strain values down to approximately  $3 \times 10^{-6}$  upon assuming Young’s modulus  $E$ , for aluminium to be  $E \approx 7.05 \times 10^{10}$  N/m<sup>2</sup>.

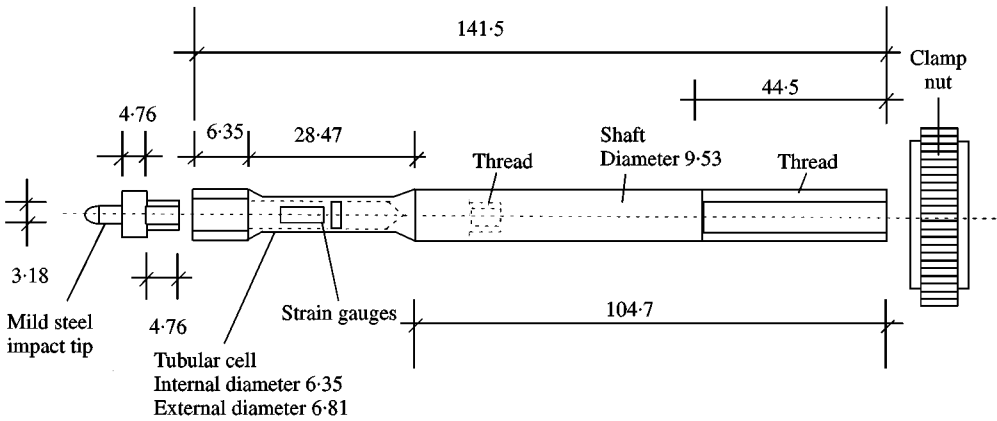


Figure 1. Schematic representation of the impact load cell apparatus. Dimensions are given in millimetres.

The load cell is made up of three distinct parts. A solid 9.53 mm diameter aluminium rod threaded at the fixed end (right-hand side in Figure 1) which is used to attach the cell to the experimental rig held in place with the clamp nut. The load-sensing cell consists of a thin-wall aluminium tube which is screwed into the free end of the solid rod. Four SHOWA N11-FA-2-120-23 electronic resistance strain gauges (ERSG) are bonded onto the outside of the tube wall, two primary gauges mounted longitudinally, and two secondary gauges circumferentially to form an active four-arm bridge. A PTFE (plastic) sleeve which slides over the cell protects the ERSG from external effects. The final part of the assembly is a mild steel rounded tip screwed into the free end of the tubular cell to take the impact force.

The ERSG bridge is supplied with a stabilized 7 V supply from a conditioning unit which also contains a high-gain stable amplifier. The gain may be varied and, for this particular application, has been adjusted to  $\times 770$ . A high gain is necessary since at a load of 1 N, the bridge output is of the order of only 20  $\mu\text{V}$ . The load cell was calibrated, and found to have a linear sensitivity of 21.8 mV/N over a range of 0–3.14 N.

The beam itself has dimensions  $332 \times 25 \times 3$  mm. Assuming a Young's Modulus for mild steel of  $205 \times 10^9$  N/m<sup>2</sup>, and a density of 8500 kg/m<sup>3</sup>, one can calculate that the first and second natural frequencies of the beam are approximately 22 and 135 Hz respectively. The load cell is mounted perpendicular to the beam at a point close to the tip, this can be seen in the photograph shown in Figure 2. The output from the load cell was recorded using an SGA800 strain-gauge monitor, linked to a personal computer. An initial gap was set between the beam and the load cell, and this is referred to as the *stop distance*. This distance was fixed at a value which corresponds approximately to 0.092 V from the beam displacement transducer. The beam was forced harmonically by using a magnetic forcing transducer, which had a fixed forcing amplitude of approximately 0.15 V. The forcing frequency can be varied as required. For this particular configuration of the load cell and beam vibro-impact motion (only) occurs for forcing frequency values close to the first

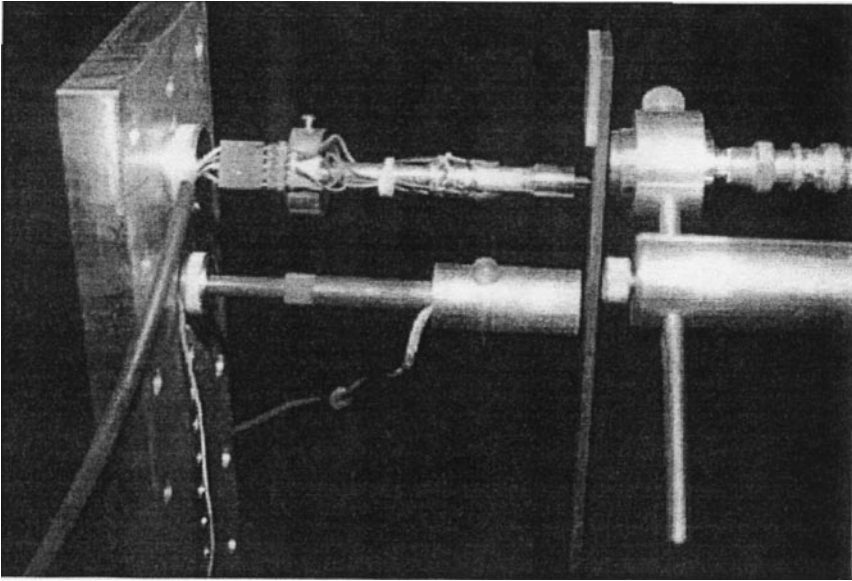


Figure 2. Impact load cell positioned in cantilever beam-experimental apparatus.

natural frequency in the range (of approximately)  $19.0 < f < 24.5$  Hz, where  $f = 1/T$  and  $T$  is the period of forcing.

### 3. RECORDING SPIKE DATA

In this section the techniques used to record the impulse spike data from the load cell are described. The voltage signal  $b(\tau)$ , where  $\tau$  is time, from the strain-gauge monitor was digitally sampled and recorded by using a National Instruments LabPC + data-acquisition board and Labview 4.0 software installed on a personal computer. The maximum sample rate  $R$ , we were able to achieve using this configuration was  $R = 60\,000$  samples/s. Figure 3(a) shows a data sample (or time series) recorded using this sample rate, where  $b(\tau)$ , strain is plotted against time  $\tau$ . Similar data from a mechanical experiment has been shown in reference [14]. At this rate of sampling, recording  $N = 5000$  samples corresponds to 0.08 s of data. The sample contains one impulse spike, the remaining data being noise generated in the electronic circuitry used for instrumentation and from external disturbance/vibration of the system.

#### 3.1. SAMPLE RATE

A close up of the impulse spike is shown in Figure 3(b) (where the individual sample values are shown as diamonds). The spike rises very quickly to a peak, and has a more gradual decay which contains additional oscillatory components, possibly caused by reflected waves in the load cell and/or relaxation of the strain

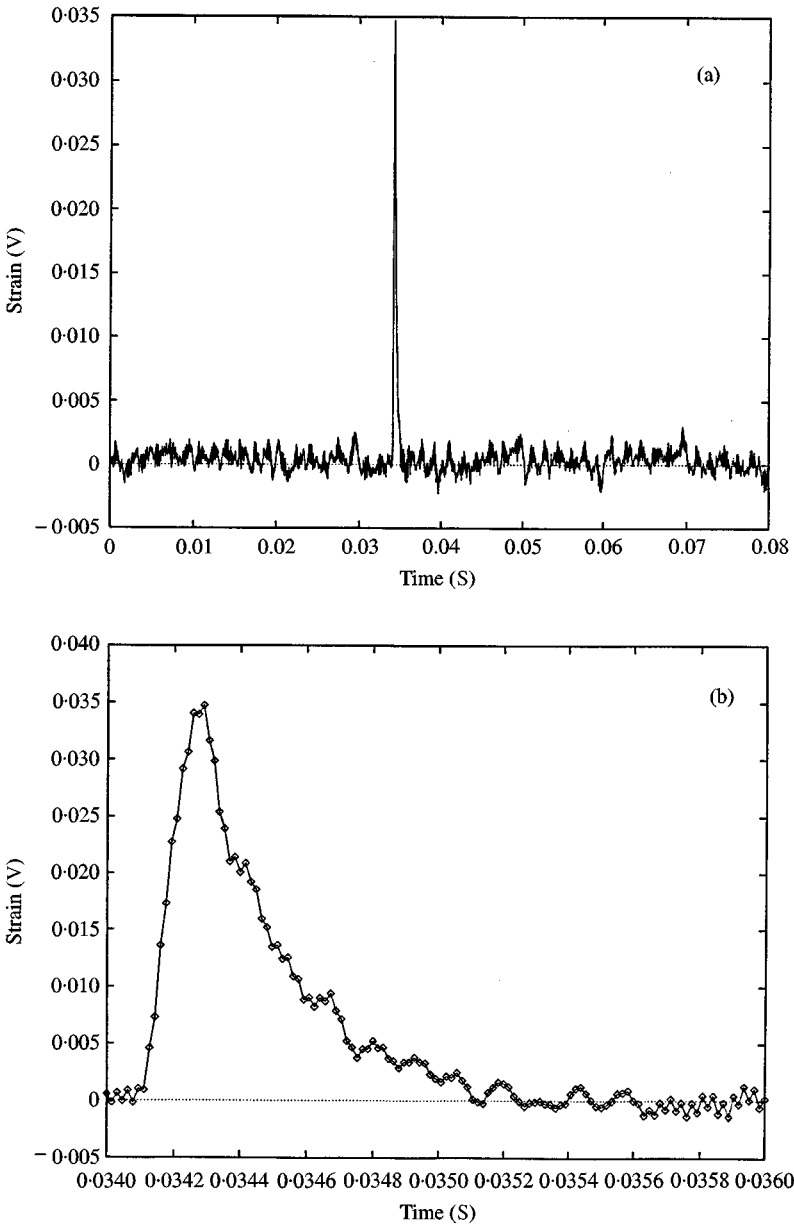


Figure 3. Time series of a vibro-impact motion showing response of impact load cell  $b(\tau)$  as strain in volts using a sample rate of 60 000 samples/s: (a) 5000 samples, (b) 120 sample close up of impulse spike, individual samples shown as diamonds.

gauges. The number of samples  $S \approx 90$  recorded while the beam is in contact with the constraint may be determined from Figure 3(b). It follows that the time of contact  $\tau_c$  is related to the sample rate by the relation  $\tau_c = S/R$ . Thus, one can choose an appropriate sample rate  $R$  from the time of constant  $\tau_c$ , such that one can achieve a desired number of samples per spike. Setting  $R \leq 1/\tau_c$  means that the

interval between samples  $\Delta\tau$  is large enough for whole spikes to be missed. Therefore, the minimum sample rate must be higher than this value, at least double, and the ideal rate, significantly higher, depending on the application. However, sampling at very high sampling rates has the disadvantage that large amounts of data are recorded for relatively short time spans. In addition for spike data, most of the signal is noise, the spikes constitute only a small part, and therefore most of the data recorded is actually unwanted. For example, the data shown in Figure 3,  $N = 5000$  and  $S = 90$ , and therefore approximately 4910 points or 98.2% of the data is noise. One can overcome this problem by using thresholds, which is discussed in section 3.2.

The sampling rate also has a significant effect on the peak value of the impulse spike. Because the spikes rise and fall so quickly, it is quite easy for the peak *recorded* value to be some way from the actual peak value. Therefore, an attempt to balance the need for accuracy and using excessive computing power must be made. For data which is to be used for quantitative analysis, such as the calculation of impact forces, we have used a sampling rate of  $R = 50\,000$ , for qualitative data lower sampling rates have been used.

### 3.2. THRESHOLD VALUES

To avoid recording excessive quantities of unwanted data one can define a *threshold value*  $H$  to distinguish between unwanted data (noise) and wanted data (impulse spikes), such that  $b(\tau) > H$  is recorded, and  $b(\tau) < H$  is disregarded. For example, for the data shown in Figure 3, a threshold value of  $H = 0.005$  could be chosen to distinguish between noise and spike data. This choice is arbitrary, and can lead to the following scenarios: (1) threshold value too high, low-velocity impacts will be missed; (2) threshold value too low, noise peaks may be mistaken for impulse spikes.

Experimentally another problem encountered is that of zero-offset drift, where the strain-gauge monitor of zero offset changes slowly during an experiment, causing the threshold value to effectively change. We define these problems collectively as *spike identification*. Other possible methods of identifying spikes are averaging-type processes [13], or the imposition of an additional threshold value on  $S$ , such that a  $S$  must be greater than a certain minimum threshold value before  $b(\tau) > H$  constitutes a spike. However, these processes are just different ways of choosing arbitrary threshold values, so which method is used again depends on the application. The effect of choosing threshold values will be discussed further in section 5.

## 4. EXPERIMENTAL RESULTS

### 4.1. THE BEAM-STOP SYSTEM

In general, periodic impacting motion is denoted period  $(p, q)$  where  $p$  impacts occur in  $q$  forcing periods. From previous experimental observations [4] for the cantilever beam system, we know that periodic vibro-impact motion where one

impact occurs in one period of the forcing, is predominant for this cantilever beam system. We refer to such motion as period (1, 1) motion and show a typical time series of the beam motion and the impact load-cell response, Figure 4, as voltage output from respective transducers/gauges.

The impulse spikes can be seen to coincide with the minima of the displacement curve (dashed line Figure 4), where impacts occur. The amplitude of these displacement minima correspond approximately with the stop distance, 0.092 V. Figure 4 demonstrates qualitatively the connection between the motion of the beam and the response of the load cell. In the remainder of this work we consider the dynamics of the system using the signal from the load cell (impact stop) alone, although we assume that we know the forcing frequency  $f$  of the system.

We now consider a set of spike trains, or time series, recorded in the frequency range  $21.5 < f < 24.5$ . Four of these recorded time series are shown in Figure 5. All the motions recorded here are period (1, 1) motions which can be seen from the regular spacing of the spikes. Although other periodic and non-periodic motions can occur for this beam [4], they occur in a very small frequency range, approximately  $19.0 < f < 20.5$ , just after *grazing* has occurred. Impacts which occur just after grazing are, by their nature, of low velocity, and as a result the impulse spikes recorded with the load cell are very difficult to distinguish from the background noise. An example of a motion from this frequency range is discussed in section 5.

One can see from Figure 5 that, in general terms, the magnitude of the impulse spikes increases as  $f$  increases. The problem of spike identification can be

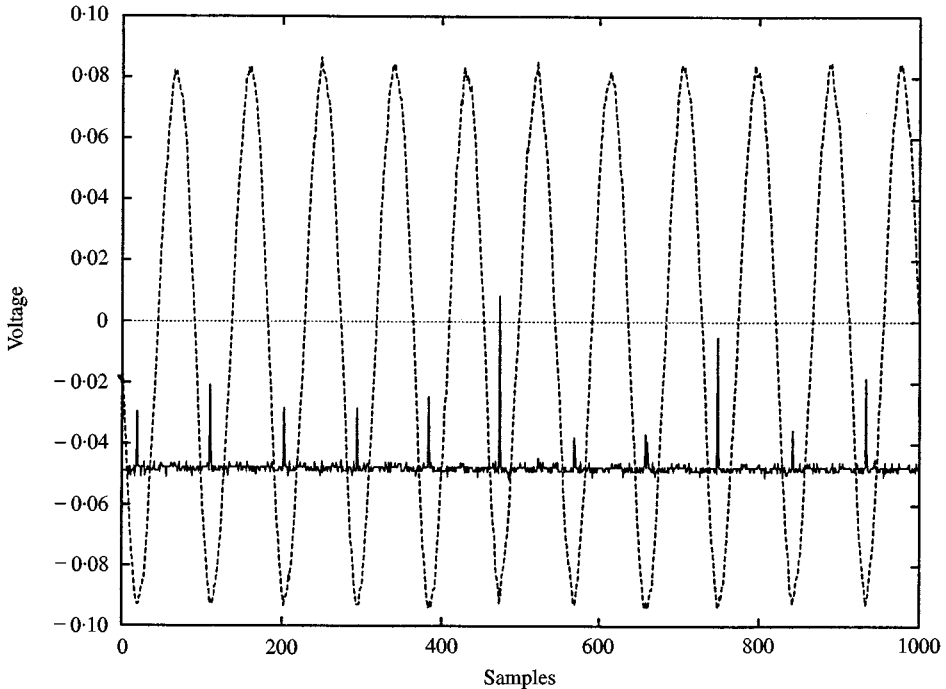


Figure 4. Time series of a vibro-impact motion showing the displacement of the beam tip (dotted line) and response at the impact load cell (solid line).

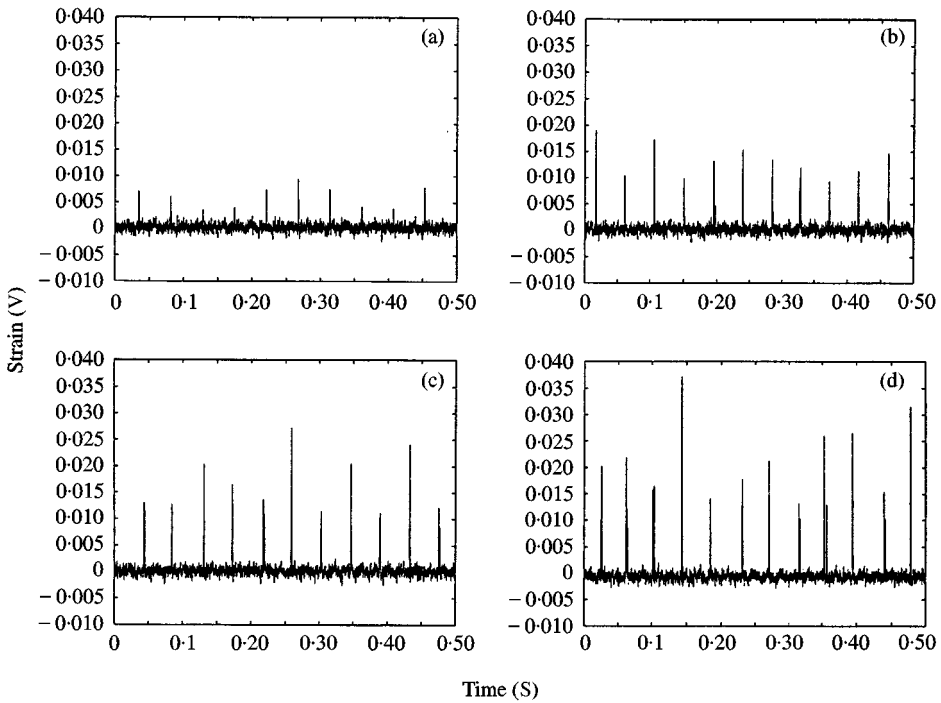


Figure 5. Time-series data recorded from impact load cell: (a)  $f = 21.5$ , (b)  $f = 22.5$ , (c)  $f = 23.1$ , (d)  $f = 24.0$ .

clearly seen in the time series in Figure 5(a), which is recorded at the lowest frequency level of 21.5 Hz. For the other time series shown in Figure 5, the impulse spikes have greater amplitudes which makes it easier to choose suitable threshold values.

One can observe that the maximum amplitude of the spikes varies significantly throughout all the time series. This may be a result of the limitations of digital sampling, mentioned in section 3.1, or modal behaviour of the beam, or a combination of both. The maximum value of the spikes appears qualitatively to rise and fall as if within some envelope frequency, similar to the beating phenomenon. As the beam is being forced close to its first natural frequency, beating may explain this behaviour, but equally it could be an *aliasing* type of behaviour, the effect of noise, or simply a modal-beam response.

In general, the cantilever beam is an infinite-dimensional dynamical system. Usually however, the dynamics of such systems reduce onto a finite-dimensional manifold within an infinite-dimensional *phase space*. Thus the finite-dimensional dynamics of the (beam) system can be described by a dynamical system of the form  $\dot{\mathbf{x}}_\tau = f(\mathbf{x}_\tau)$ , where  $\mathbf{x}_\tau = \mathbf{x}(\tau)$  is the state vector in a finite,  $k$ -dimensional phase space  $\mathbf{x} \in \mathbb{R}^k$ .

#### 4.2. TIME AT IMPACT

The introduction of a threshold provides a means of experimentally determining the time of impact and the time interval between impacts. Theoretically, one can



assume there is a limit such that when an *instantaneous* impact occurs the time the beam stays in contact with the stop tends to zero, i.e.  $\tau_c \rightarrow 0$ . This is a theoretical concept only, as any physical impact will be of some finite duration. However, assuming  $\tau_c \approx 0$  simplifies the mathematical modeling of the beam system considerably.

Using the statistical properties of the data recorded from the system one can compute the proportion of the time which the beam spends in contact with the stop: Let  $\mathcal{B}$  denote the region of phase space corresponding to the impact stop, and let  $\mu$  be an ergodic invariant probability measure describing the evolution of the physical system [15]. Then, by ergodicity,  $\mu(\mathcal{B})$  is the long-term proportion of the time that the beam spends in contact with the stop. An invariant measure value close to zero,  $\mu(\mathcal{B}) \ll 1$  corresponds to the system spending a small amount of time in  $\mathcal{B}$  (i.e. at the impact stop). Thus, one can quantify the assumption made in the study by using the instantaneous model that the physical contact time  $\tau_c$  is “short” compared to the time between impacts [4].

Let  $\{\mathbf{x}_\tau\}$  denote the evolution of the (beam) system in phase space, so that the voltage stream (recorded at the stop) is given by  $b(\tau) \equiv b(\mathbf{x}_\tau)$ . Consider the time series from the load cell to have a sequence of *firing times*  $T_0, T_1, T_2, \dots, T_n$  corresponding to the discrete voltage signal  $b(\tau_k)$  crossing the threshold  $H$  with positive slope, such that  $b(\tau_k) > H, b(\tau_{k-1}) < H$ . Thus,  $\mathcal{B} = \{\mathbf{x} : b(\mathbf{x}) \geq H\}$ . Assume that time is scaled such that  $T_0 = 0$ , then  $T_n$  is the total time of the signal. After each firing time,  $T_j$ , an impulse spike occurs with duration  $s_j$  above the threshold  $H$ , such that  $b(\tau) > H$  (i.e.  $s_j \approx \tau_c$  for spike  $j$ ). The *contact time* measure  $\mu_H$  can be defined as

$$\mu_H = \mu(\mathcal{B}) = \lim_{t \rightarrow \infty} \frac{1}{t} \int_{t=0}^t \chi_{\mathcal{B}}(\mathbf{x}_\tau) d\tau \approx \frac{1}{T_n} \int_{t=0}^{T_n} \chi_{\mathcal{B}}(\mathbf{x}_\tau) d\tau, \tag{1}$$

where

$$\chi_{\mathcal{B}}(\mathbf{x}) = \begin{cases} 1 & \text{if } \mathbf{x} \in \mathcal{B}, \\ 0 & \text{if } \mathbf{x} \notin \mathcal{B}. \end{cases} \tag{2}$$

Clearly  $\mathbf{x} \in \mathcal{B} \Leftrightarrow b(\mathbf{x}) \geq H$ , so that  $\chi_{\mathcal{B}}(\mathbf{x}_\tau) = \chi_{[H, \infty)}(b(\tau))$ . Thus,

$$\mu_H \approx \frac{1}{T_n} \int_{t=0}^{T_n} \chi_{[H, \infty)}(b(\tau)) d\tau = \frac{1}{T_n} \sum_{j=0}^{n-1} s_j. \tag{3}$$

The smaller the  $\mu_H$  value, the closer the real system is to a short duration impact.

The time of contact measure computed for the cantilever beam system for the frequency range  $21.5 < f < 24.0$  is shown in Figure 6. At each frequency setting an impulse spike time series was recorded (data shown in Figure 5), and  $\mu_H$  computed. The maximum standard error for these computation was less than 0.00025 for all time series. From Figure 6, one sees that  $\mu_H$  increases approximately linearly with frequency. The linear increase in Figure 6 is due to the hardening spring behaviour of the vibro-impact beam system [4]. A saddle node bifurcation occurs soon after  $f = 24$  Hz, and impacting motion no longer exists. For this data all the values fall

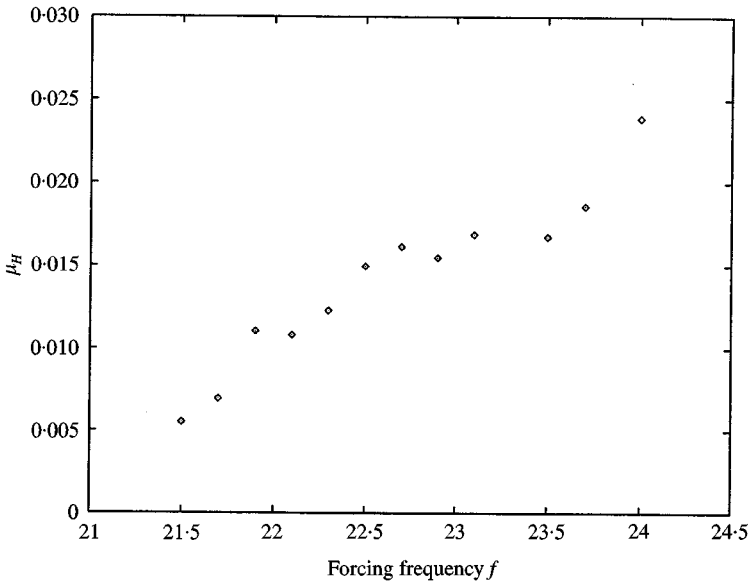


Figure 6. The time of contact measure  $\mu_H$  for the cantilever beam system.

below approximately 0.025, which implies that for all motions the time spent in contact with the stop is less than 2.5%. In view of the conclusion from reference [4] that the instantaneous impact rule models the dynamics of the system adequately, one can postulate that for systems with an *contact time* invariant measure  $\mu_H \leq 0.025$  an instantaneous impact rule is a valid approximation when modelling the system. In addition, one concludes that systems where  $\mu_H \leq 0.025$  have short impacts.

Also one can note that this approximation is better for lower-frequency values, presumably because the impact forces (discussed in section 4.4) are lower. The relation between the beam-system dynamics  $\mathbf{x}_\tau$  and the voltage signal  $b(\tau)$  is discussed further in section 5 where reconstructing the dynamics of the beam  $\mathbf{x}_\tau$  by using the signal  $b(\tau)$  is considered.

#### 4.3. MULTIPLE IMPACT SPIKES

An interesting phenomenon observed from the data is the occurrence of *multiple* impact spikes. By this we mean two or more spikes which occur very close together, such that on the scale shown in Figure 5 they may appear as a single spike. For period (1, 1) motion where the beam is forced at a frequency  $f$ , the time between impacts is approximately the period of the forcing such that the interspike interval  $I \approx 1/f$ . As impacting motions exist only around the first natural frequency of the beam, all motions are dominated by the response of the first mode and are hence predominately period (1, 1). However, the occurrence of impacts induces contributions to the response from higher modes of vibration. As a result, multiple

spikes will occur close to the periodic time of impact,  $\text{mod}(\tau_i) \approx \text{constant}$ ,  $i = 0, 1, 2, 3, \dots, n$  for periodic motions. Thus, a group of individual spikes forming a multiple spike lies within some small time perturbation  $\varepsilon$ ,  $\varepsilon \ll 1$  of  $\tau_i$ ,  $\tau_i \pm \varepsilon$ . Other spikes which occur in the remaining interval  $(\tau_i + \varepsilon, \tau_{i+1} - \varepsilon)$  are referred to as *spurious* spikes, whether caused by an impact or noise.

As an example of multiple spikes, consider the time series shown in Figure 5(d). The forcing frequency for this test was  $f = 24$  Hz, so the period of forcing is  $1/f \approx 0.04167$  s which one expects to be approximately equal to the period of the response and hence the interspike interval  $I$ , such that  $I \approx 1/f$ . In Figure 7  $\tau_c$  is plotted against  $I$  for the data shown in Figure 5(d). From this figure one can see that there is a group of points around  $I \approx 0.04167$ ,  $\tau_c \approx 0.0005$ , corresponding to the period of forcing. In addition, four points grouped together have a much smaller  $I$  value, these correspond to the additional spikes which form the multiple impacts. In fact there are four double spikes in this time series, only one of which is clearly visible in Figure 5(d). For this particular example  $\varepsilon = 0.005$  would be a suitable value to define the multiple spikes. Note also that a greater number of multiple spikes occur for higher forcing frequencies. This is a direct result of the increase in higher modal activity for greater impact forces, discussed in section 4.4.

#### 4.4. MEASUREMENT OF IMPACT FORCE

The measurement of impact forces has important applications in engineering systems where components are subject to impact loading. One can obtain discrete values of the impact force,  $F(\tau)$ , directly from the voltage signal  $b(\tau)$  by using

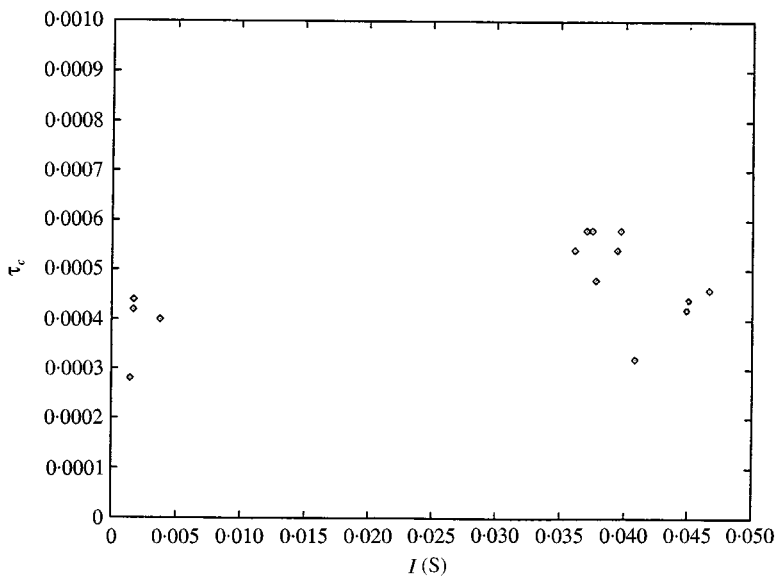


Figure 7. Contact time  $\tau_c$  versus interspike interval  $I$ .

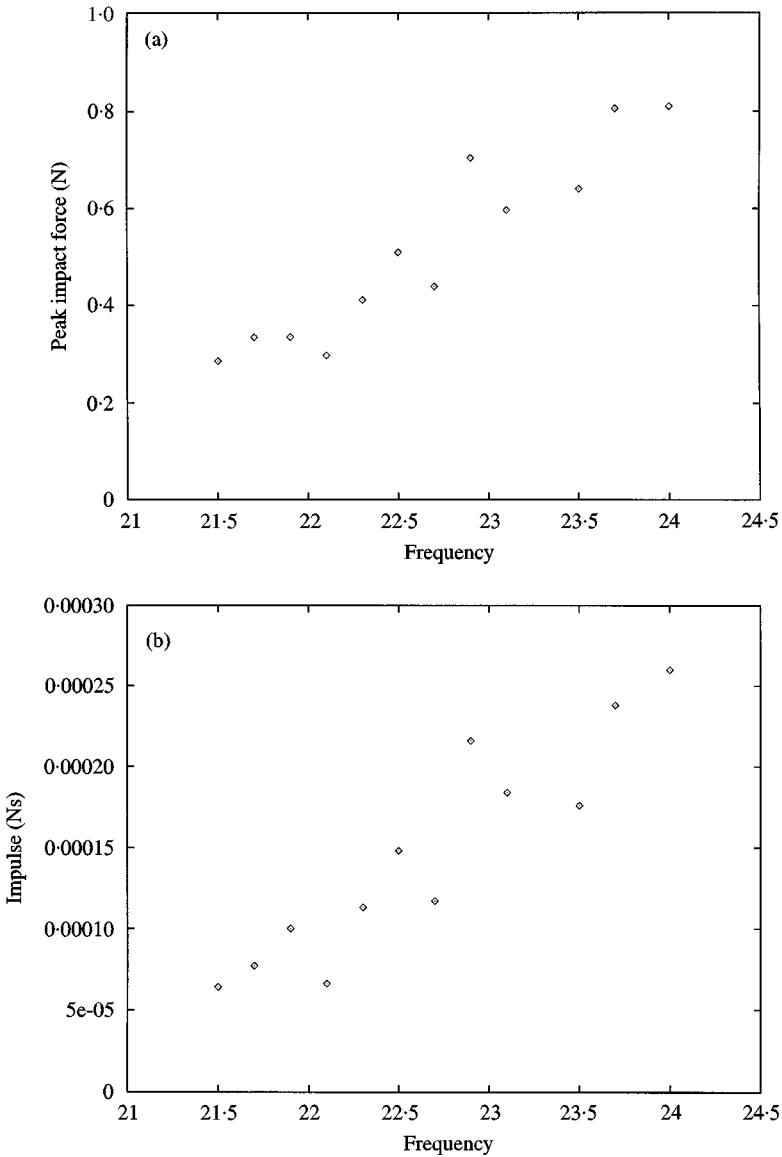


Figure 8. Computation of impact forces using the time-series data shown in Figure 5: (a) average peak-impact force value, (b) average impulse value for each time series.

the calibration constant  $b(\tau)/F(\tau) = 21.8 \text{ mV/N}$ . In Figure 8(a) the computed average peak impact force over each of the time series shown in Figure 5. This has been computed by recording the maximum value for each spike in the time series, and then computing the mean value. The peak impact forces for the recorded time series are in the range 0.2–1.0 N and appear to increase approximately linearly with increasing frequency. As with the time of contact, the linear increase is due to the hardening spring behaviour of the impacting beam system [4].

In addition to computing the peak impact force, one can compute the change in momentum for each impact by using the impulse momentum law [16],

$$mv_i(\tau_{i-}) - mv_i(\tau_{i+}) = \int_{\tau_{i-}}^{\tau_{i+}} F(\tau) dt, \quad (4)$$

where  $m$  is the (lumped) mass (of the beam),  $v_i(\tau_{i-})$  is the velocity at the start of the impact at time  $\tau_{i-}$ ,  $v_i(\tau_{i+})$  is the velocity at the end of the contact time  $\tau_{i+} = \tau_{i-} + \tau_c$ , where  $\tau_c$  is the duration of the contact interval.  $F(\tau)$ , for  $\tau_{i-} < \tau < \tau_{i+}$ , represents the force applied by the mass to the impact stop. Thus, by computing the integral on the right-hand side of equation (4) (as a discrete approximation) one can estimate the change in momentum during impact. This computation has been done for the time series shown in Figure 5, and the results are shown in Figure 8(b), where the average value of impulse for each time series is plotted. As with peak impact force there is an approximately linear increase of impulse with frequency value.

For impacting systems, the change in momentum during impact can be related to the coefficient of restitution via the coefficient of restitution rule

$$v_i(\tau_{i+}) = -rv_i(\tau_{i-}), \quad (5)$$

where  $r$  is the coefficient of restitution with a value in the range  $r \in [0, 1]$  depending on the material properties of the system. Combining equations (4) and (5) one obtains the relation

$$m(1+r)v_i(\tau_{i-}) = \int_{\tau_{i-}}^{\tau_{i+}} F(\tau) dt. \quad (6)$$

This expression analytically represents the relationship between the beam and stop because the velocity of the beam tip  $v_i \in \mathbf{x}$ , and  $b(\tau)$  is a function of the impact force  $F(\tau)$ . Assuming that the impact law is instantaneous, as in section 4.2, implies that  $F(\tau)$  is a Dirac delta function, with an amplitude related to the peak force of the impact. This assumption can be made when considering the global dynamics of the system, such that the contact time measure  $\mu_H \ll 1$  as discussed in section 4.2. For single impact analysis, for example Figure 3(b) where  $\mu_H \approx 1$ , alternative functional forms for  $F(\tau)$  will be more suitable. If additional experimental measurements are available from the system, equation (6) can be used to obtain an estimate of either the impact velocity or coefficient of restitution for the beam system.

## 5. RECONSTRUCTING DYNAMICS USING INTERSPIKE INTERVALS

One can now consider reconstructing the dynamics of the system by using *interspike intervals*. The concept of reconstructing the dynamics of a system using time-series data was first introduced by Takens in reference [17], and a general review of the subject is given by Broomhead and King in reference [18]. The application of these techniques to interspike intervals was carried out by Sauer in reference [13]. Essentially, it is assumed that the time-series signal is generated by an underlying dynamical system. For our beam system we assume that this

dynamical system is deterministic with an additional noise component. As a result the time signal can be rewritten  $b(\tau) = \hat{b}(\tau) + \xi$ , where  $\hat{b}(\tau)$  is the deterministic part of the signal, and  $\xi$  corresponds to noise [18]. For this type of data, the method of delays [17] or singular systems analysis [18] can be implemented to reconstruct the underlying dynamics of the system. By underlying dynamics, we mean reconstructing the *attractor*  $\mathcal{A}$ , on which the trajectories of the dynamic system converge for a particular set of parameter values.

### 5.1. INTERSPIKE INTERVALS

When using interspike intervals to reconstruct the dynamics of the system, one assumes that the only information is the sequence of firing times  $T_i, i = 0, 1, 2, \dots, n$ , and from this one can construct a sequence of interspike intervals  $I_i, i = 0, 1, 2, \dots, n$ . The firing times can be obtained either by *integrate and fire* [13] or by threshold crossing, as for our data. In reference [13] it was demonstrated (numerically, without noise) that the reconstruction of the dynamics can be achieved for a deterministic non-linear system by using the method of delays applied to interspike intervals obtained by using the integrate and fire technique. The firing times for our system are obtained via the threshold crossing method indirectly: i.e., no direct measurements of the beam system are required.

As mentioned in section 4.1, the cantilever beam is an infinite-dimensional dynamical system with dynamics which reduce onto a finite-dimensional manifold in phase space. In fact, it was concluded in reference [4] that a *single-degree-of-freedom* model was sufficient to model qualitative dynamics of the system. Thus the finite-dimensional dynamics of the (beam) system  $\mathbf{x}_\tau, \mathbf{x} \in \mathbb{R}^k$ , are related to the voltage measurements at the load cell such that,  $b(\tau) = \mathbf{F}(\mathbf{x}_\tau)$ , where  $\mathbf{F}: \mathbb{R}^k \mapsto \mathbb{R}$ , is the *measurement function* [19].

Having computed the firing times for a particular time series, one can depict them as a spike train. Two spike trains computed from load-cell data are shown in

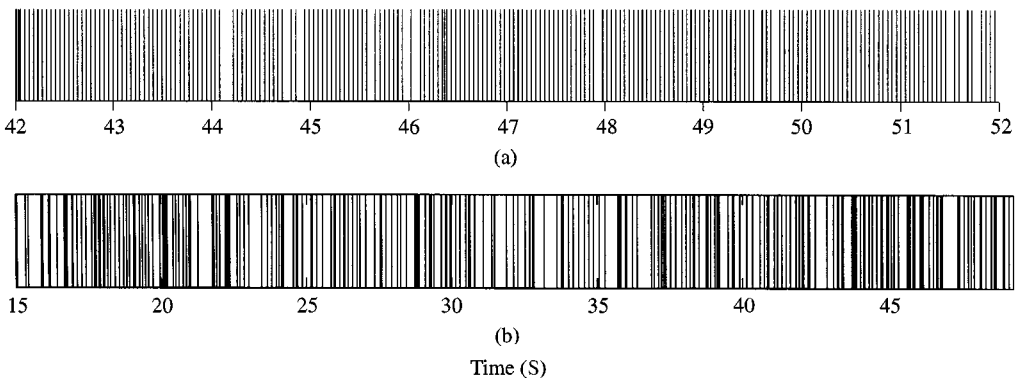


Figure 9. Schematic representation of a spike train computed from a load-cell signal: (a)  $f = 22.1$ , (b)  $f = 20.1$ .

Figure 9. This gives a qualitative representation of the signal which one can now use to reconstruct the dynamics. Note also that, this type data could be recorded *directly* from a system, for example by using an electrical contact, in which case the interspike interval method would be the only way of gaining insight into the system behaviour.

## 5.2. DELAY RECONSTRUCTION

One can reconstruct the dynamics by using the method of delays [13, 17, 18] by introducing a delay vector of inter spike intervals  $\{I_i, I_{i-1}, \dots, I_{i-m+1}\}$ , where  $m$  is the *embedding dimension*. Castro and Sauer [20] demonstrated that the correlation dimension  $d$  of the attractor  $\mathcal{A}$ , can be found by using interspike intervals (integrate and fire). In addition, the authors have postulated that estimating the dimension when using threshold generated intervals would give the dimension of the attractor in a  $(d - 1)$ -dimensional space. This is true when recording the times trajectories intersect with a threshold, which is qualitatively the same as taking a  $d - 1$  Poincaré section through the flow. For impacting systems, recording the time of impact is qualitatively the same as recording the times of intersection of the system trajectories with a hypersurface  $\Sigma$  denoting the position of the impact stop. The mapping  $\Sigma \mapsto \Sigma$  is now known as the *impact map*, following the work of Shaw and Holmes reference [6]. Essentially one is recording these times via the load-cell signal  $b(\tau)$ . Thus if one reconstructs the dynamics of the system, it will be the dynamics in  $\Sigma$ , essentially that of the impact map.

Two recorded samples of interspike interval data from the load cell are shown in Figures 10(a) and (b) (which correspond to the spike-train data shown in Figure 9). A clear banded structure can be seen in both these plots, corresponding to multiples of the forcing interval, which we define as  $\bar{T} = 1/f$ . The correlation dimension  $d$  can be estimated by using the method proposed by Grassberger and Procaccia in reference [21]. Figures 10(c) and (d) show a  $\ln$ - $\ln$  plot of the correlation dimension versus the  $\varepsilon$  radius used to compute it. Three sets of data are shown corresponding to  $m = 1$  (diamonds),  $m = 2$  (crosses),  $m = 3$  (boxes). In Figure 10(a) one can see that most of the data is concentrated at the value  $\bar{T} = 0.0452 \approx 1/22.1$ . Hence in Figure 10(c), there is near-complete correlation,  $\ln(d) = 0$ , until  $\varepsilon$  reduces below this value (another threshold type effect, which occurs at  $-\ln(\varepsilon) \approx 3.09$ ), after which the correlation becomes approximately constant with zero slope, before a final sharp upturn. This final upturn is due to the band of data very close to zero, caused by multiple spikes. The data in Figure 10(b) occurs at banded intervals of,  $\bar{T} = 0.0498 \approx 1/20.1$ , but many more bands are apparent than the data in Figure 10(a). Thus, the correlation dimension for this data, Figure 10(d), has a more gradual transition between complete correlation and constant correlation with zero slope. There is no final upturn in this data due to a much smaller proportion of the data being close to zero. Thus for a fixed-point attractor, one would expect  $d = 0$ , which appears to be the case for both sets of data.

The correlation dimension for the attractor  $\mathcal{A}$  is taken to be the slope of the linear part of the  $\ln$ - $\ln$  plot. This is open to some interpretation, as can be seen in Figures 10(e) and (f) where the slope is plotted against  $-\ln \varepsilon$ . From these plots one

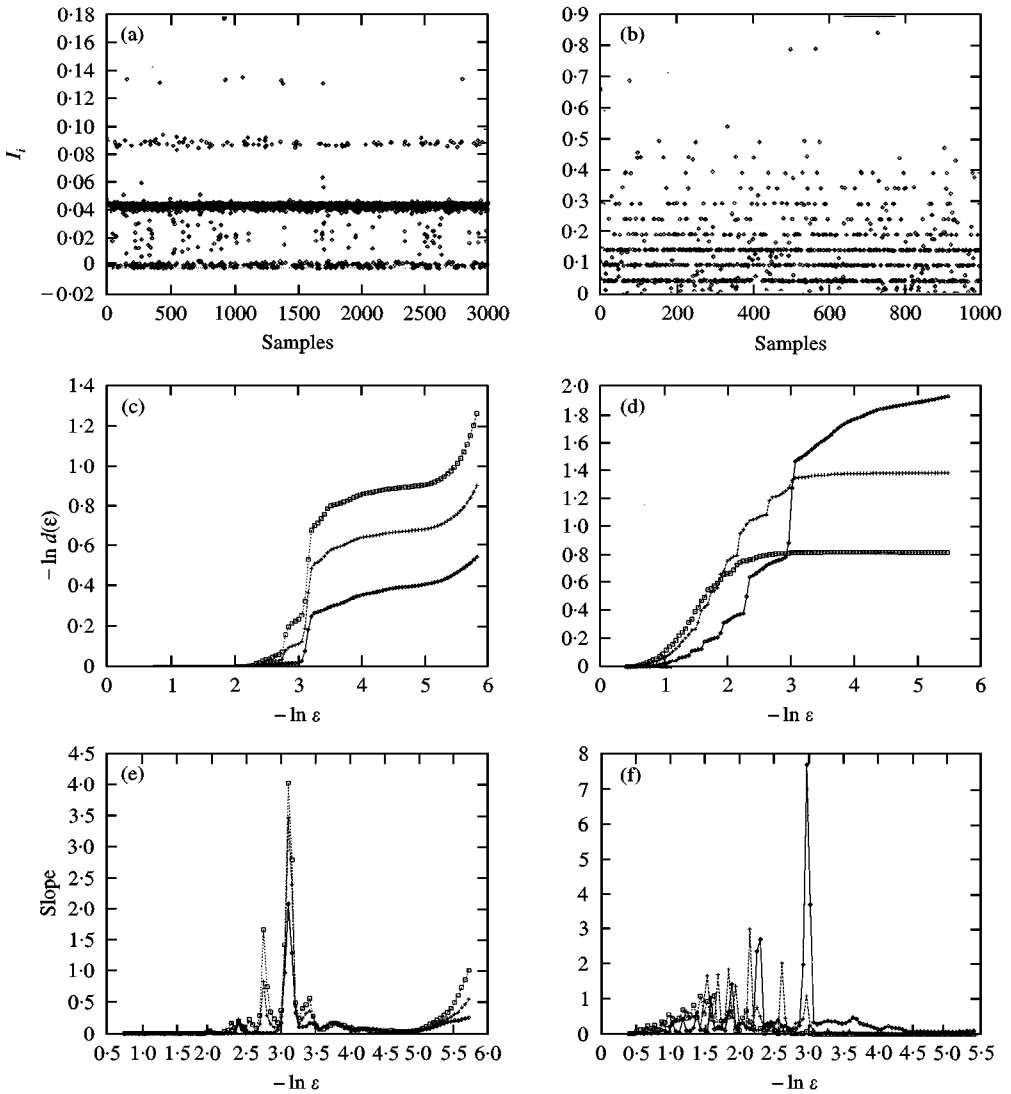


Figure 10. Interspike interval data: (a)  $f = 22.1$  and (b)  $f = 20.1$ . Estimation of correlation dimension (c) and (e) for data in (a), (d) and (f) for data in (b). Data sets:  $m = 1$  (diamonds);  $m = 2$  (crosses);  $m = 3$  (boxes).

can see that as the radius becomes small  $\epsilon \rightarrow 0$ , the correlation dimension for both sets of data  $d \rightarrow 0$ . The data we have analysed comes from periodic vibro-impact solutions of the beam, which will have fixed-point attractors in the impact map,  $\Sigma$ , of dimension zero.

From embedding theory, the dynamics of the sequence of intervals can be reconstructed in  $\mathbb{R}^m$  were  $m \geq 2d + 1$ . So for our data,  $d \approx 0$ , so  $m \geq 1$ , and we reconstruct the dynamics using a simple delay plot in  $\mathcal{R}^2$ .

The delay plots from the load cell data are shown in Figure 11. The data in Figure 11(a) was recorded at  $f = 22.1$  where period (1, 1) motion exists, so that all the intervals should be approximately equal. However, one can see that instead of



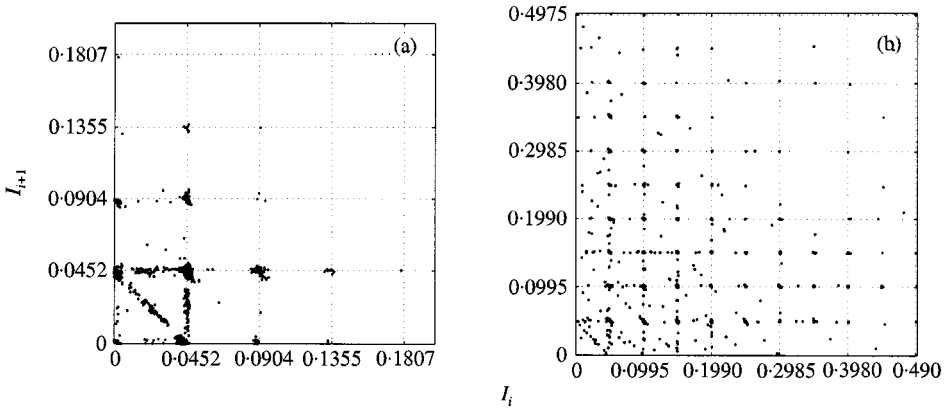


Figure 11. Experimental interspike interval delay plot: (a)  $f = 22.1$ , (b)  $f = 20.1$ .

a single (fixed) point the data is distributed over a lattice of squares with size approximately  $\bar{I}$ . Similar data has been shown in reference [22] in connection with neural firing events. The lattice structure is caused by a combination of disturbance effects. Noise recorded as part of the signal combined with limitations in the spike identification process (section 3), results in some spikes being missed completely, and some spurious spikes recorded. In addition, the multiple spike phenomena discussed in section 4.3 contributes to the distribution of points in the figure.

One can understand these effects by considering an undisturbed (ideal) period one motion with all intervals exactly equal,  $I_i = \bar{I}$  for all  $i$ . Thus with no disturbance effects, there will be a single point in the delay plot at  $(\bar{I}, \bar{I})$ . The effect of missing a spike is to produce a point at  $(\bar{I}, 2\bar{I})$ , and on the subsequent iteration at  $(2\bar{I}, \bar{I})$ . Similarly for  $p$  missing spikes points occur at  $(\bar{I}, p\bar{I})$ , and  $(p\bar{I}, \bar{I})$ . Thus, points are reflected in the line  $I_{i+1} = I_i$  giving rise to the lattice-type data structure. The probability of missing  $k$  consecutive spikes decreases exponentially with  $k$ , thus less points accumulate at intervals greater than  $\bar{I}$ . Lontin and Racicot [22] refer to the spike-missing process as *skipping*.

The effect of spurious spikes is that an interval  $a\bar{I}$  occurs, where  $0 < a < 1$ . Due to the reflective properties of the delay plot, this causes bands of points forming a triangle in the first lattice square  $(0, 0)$ ,  $(0, \bar{I})$ ,  $(\bar{I}, \bar{I})$ ,  $(\bar{I}, 0)$ . Multiple spikes correspond to points close to  $I = 0$  which can be seen clearly in Figure 10(a) and (b) (or the origin in Figure 11).

### 5.3. NUMERICAL SIMULATION

One can further understand these effects by considering a numerical simulation of the experimental data. This can be done by simulating the motion of the beam by integrating the equation of motion for a single-degree-of-freedom impact oscillator [6]. First, (white) noise is added to the numerically generated signal, and the effects of missing spikes and spurious spikes included by using random probability. Using the beam equations with added noise, one can produce the delay plot in Figure 12(a). The effect of missing spikes was simulated by randomly deleting firing

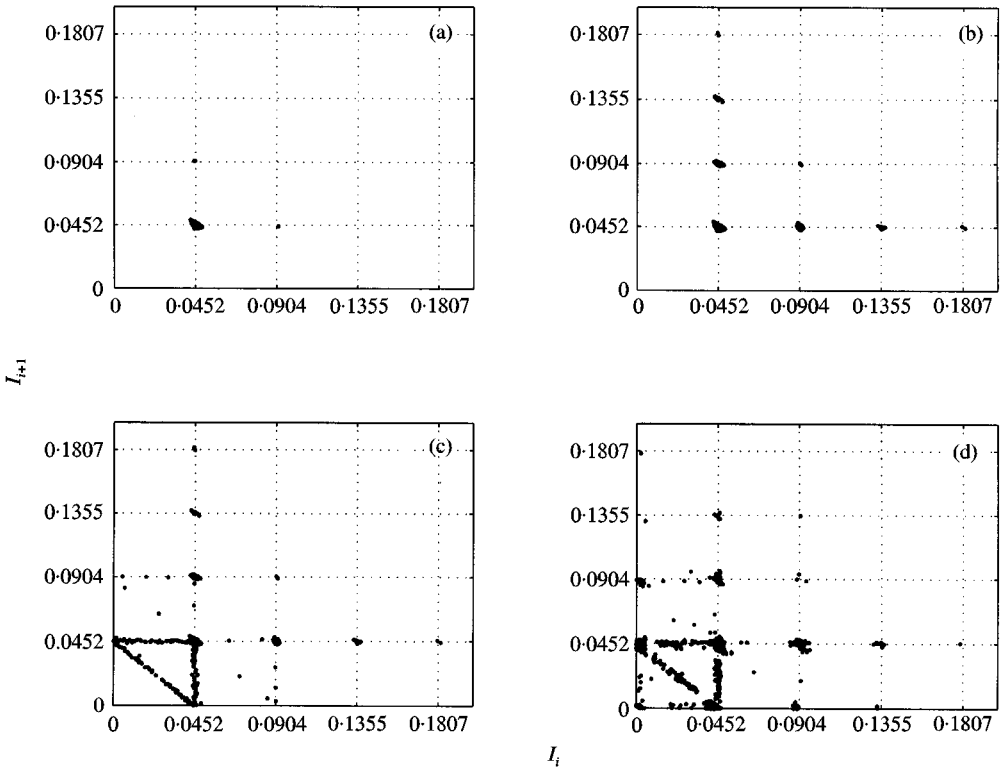


Figure 12. The effects of the data-acquisition process on experimental results. Numerical signal; (a) with added noise; (b) with noise and missed spikes; (c) with noise, missed and spurious spikes. (d) experimental data. Numerical data obtained by integrating  $\dot{x} + 0.14\dot{x} + x = 0.26 \cos(0.9822t)$  for  $x < 1.0$ , and  $\dot{x}(t_+) = -0.2\dot{x}(t_-)$  at  $x = 1.0$ . All quantities are non-dimensional;  $t = 141.37\tau$ , and an over dot represents differentiation with respect to  $t$ .

times using a 5% probability, the effect of this can be seen in Figure 12(b). Here, apart from the main concentration seen before, there are some other, smaller ones, evenly spaced at multiples of  $\bar{I}$ . The effect of spurious spikes, is demonstrated in Figure 12(c), times between actual impacts have been added using a 1% probability. The result in the plot is the horizontal, vertical and diagonal of bands of point dots visible in the figure. Finally, in Figure 12(d) the experimentally recorded data are shown, which closely match the numerical simulation. The effect of multiple spikes, can be seen as a series of points with small interspike interval values  $\ll \bar{I}$ , close to the axes of the plot. Thus one can see that using the method of delays on such data results in a highly complex plot due to a combination of noise in the system, and the data-acquisition process.

#### 5.4. PROBABILITY DENSITIES

An alternative method for analysing interspike data is to consider the *probability density* of the interspike intervals  $\rho(I)$ . To illustrate this the probability density for the examples shown in Figure 11 is plotted in Figure 13. From Figure 13(a) it is

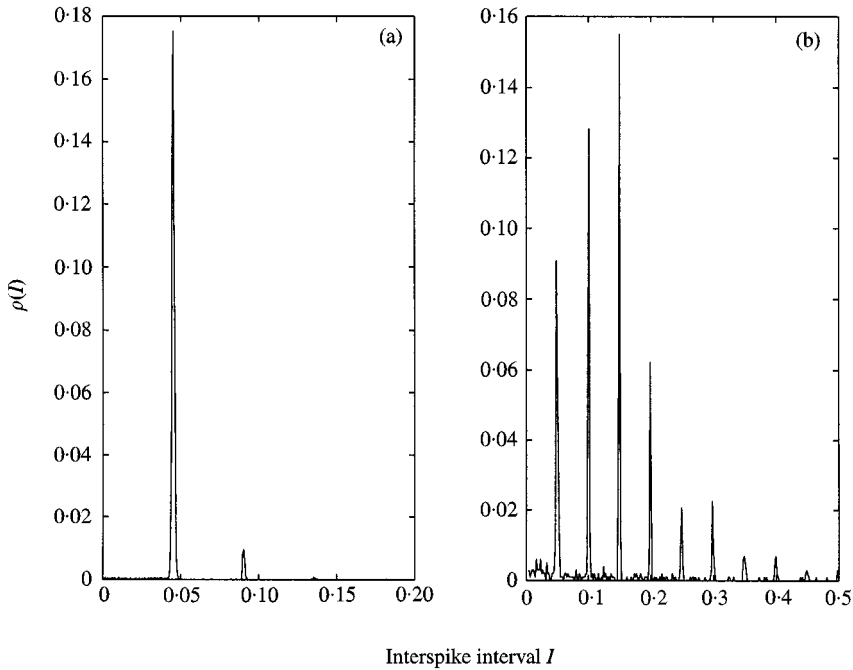


Figure 13. Probability density (histogram) of interspike interval: (a)  $f = 22.1$ , (b)  $f = 20.1$ .

clear that for the data shown in Figure 11(a) the majority of the points occur around the  $\bar{T} \approx 0.0452$  interval, and that the underlying dynamical motion is period (1, 1).

One can use this method to interpret period (1,  $q$ ) motions; i.e., the motion is still period one with respect to the number of impacts, but period  $q$  with respect to the forcing period. Thus, one would expect an interspike interval of approximately  $q/f$ , which can be recognised from the probability density plot which will be qualitatively similar to Figure 13(a). Period ( $p$ ,  $q$ ) motions where  $p$  impacts occur in  $q$  forcing periods can also be recognised. If the interval between impacts is not equal. For example, a period two motion will have two intervals (and two impacts) in two forcing periods, and thus two main values (peaks) of  $\rho(I)$ . A numerical example of such a period (2, 2) motion is shown in Figure 14(a). However, if the intervals are equal (or close to being equal) this motion will appear as period one (one peak  $\rho(I)$ ) with an interval  $q/f$ .

One can now consider the motion shown in Figure 11(b). The probability density for this data is shown in Figure 13(b). From this one can see that there are several concentrations of data. These are separated by (approximately) the forcing interval  $\bar{T} = 1/f \approx 0.0498$ . This motion was recorded in the frequency range where it is possible for motions other than period (1, 1) to exist. However, as the concentrations are evenly spaced across the probability spectrum, one can deduce that this motion is in fact period (1, 1). Any other period ( $p$ ,  $q$ ) motion would produce either a series of differing intervals, or a single interval at an integer multiple of the forcing interval  $\bar{T}$ . Non-periodic motions, such as deterministic chaos, would produce a broad-band distribution of intervals. A numerical example of the probability density of interspike interval data from a chaotic signal is shown in Figure 14(b).

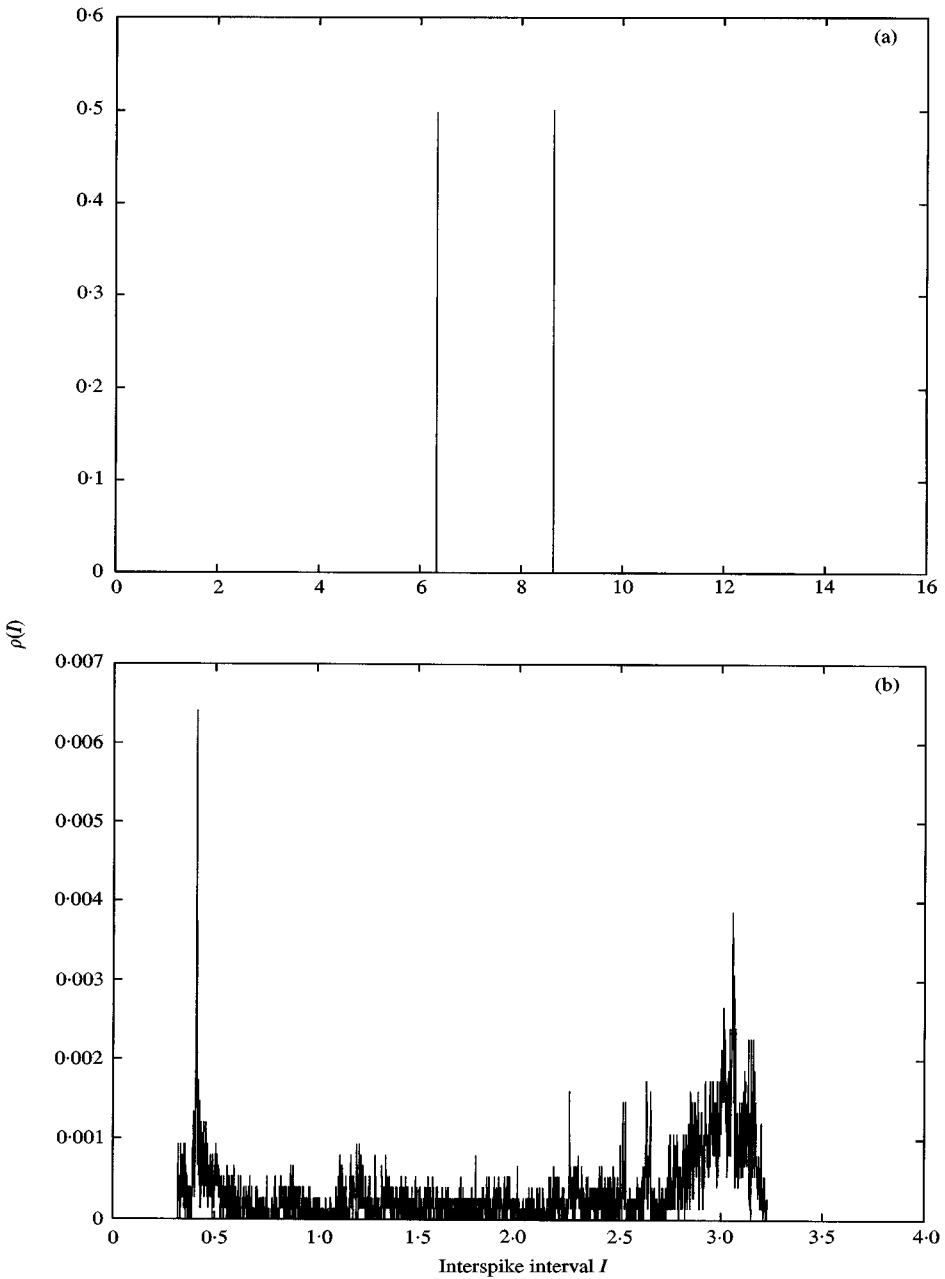


Figure 14. Numerically generated probability density (histogram) of interspike interval data. Numerical data obtained by integrating  $\ddot{x} + 2(\dot{x} + x) = F \cos(\omega t)$  for  $x < 1.0$ , and  $\dot{x}(t+) = -r\dot{x}(t-)$  at  $x = 1.0$ . All quantities are non-dimensional, and an overdot represents differentiation with respect to  $t$ . (a) period (2, 2) motion  $r = 0.7$ ,  $\zeta = 0.05$ ,  $F = 0.5$ ,  $a = 1$ ,  $\omega = 0.838687$ ; (b) chaotic motion  $r = 0.8$ ,  $\zeta = 0.0$ ,  $F = 1.0$ ,  $a = 0.0$ ,  $\omega = 2.8$ .

It is interesting to note that the motions shown in Figure 13(a) and (b) represent the same type of periodic motion, although they appear to be qualitatively different. The reason is the first spike identification problem discussed in section 3.2, namely

that the threshold value is too high, such that low-velocity impact spikes are missed. This can be deduced from Figure 13(b) by noting that the greatest  $\rho(I) = 3\bar{I}$ , indicating that the threshold has been set such that it is most likely that only every third spike will be recorded. In fact, for a frequency of 20.1 Hz all the spikes are difficult to distinguish above the background noise level. Thus in this example one is operating at the limits of these spike-identification techniques, which in practical applications is often the area of most interest.

This example clearly demonstrates the difficulties in the correct interpretation of such spike data. For systems with low-amplitude spikes (corresponding to low-velocity impacts for the beam system) the interspike interval technique is limited by the need to threshold the data, although with careful analysis information can be gained. If the spikes are well defined, one can characterize the dynamics of the system by using interspike intervals and probability densities.

## 6. CONCLUSIONS

We have considered the experimental measurement of the impulse response of a vibro-impact cantilever beam system. Recordings were taken using a specially constructed impact load cell. We have discussed the issues related to sampling impulse spike data, particularly the effects of sampling rate and threshold values.

We have used a measure of the time the beam stays in contact with the stop, to demonstrate that the instantaneous coefficient of restitution rule is a valid approximation for systems such as the beam system, also providing a measure of validity which may be used elsewhere. In addition we have considered the impact forces in the system, and highlighted the possibility of a functional link between instantaneous impact rules, and using a Dirac delta function to approximate the impact force.

In line with computational studies carried out by other authors, we have considered reconstructing the underlying dynamics using interspike intervals from experimental data. We have demonstrated for our data, that the dynamics can be reconstructed using a simple one-dimensional delay plot. The effects of noise, and the acquisition process have been simulated, demonstrating the limitations of analysing this type of data.

Finally, we have considered determining periodicity (or lack of) for different motions using probability densities. We have shown how this is possible even for data where thresholding effects have been significant during data acquisition. In addition, we have indicated how such thresholding effects can be identified using the probability-density spectrum.

This paper has presented analysis of data from an engineering system using statistical and probabilistic methods. We envisage many future applications of these type of methods to other engineering applications.

## ACKNOWLEDGMENTS

The authors would like to acknowledge the technical support given by Mr. M. Saytch in constructing the experimental apparatus and Mr. D. W. Vale for constructing the impact load cell, both in the Civil & Environmental Engineering

Department of University College London. David Wagg gratefully acknowledges the support of the EPSRC. The authors would also like to thank Rua Murray and Mike Davies for their constructive comments regarding this work.

#### REFERENCES

1. F. C. MOON AND S. W. SHAW 1983 *International Journal of Non-Linear Mechanics* **18**(6), 466–477. Chaotic vibrations of a beam with non-linear boundary conditions.
2. M. G. THOMPSON, S. R. BISHOP AND S. FOALE 1994 *Machine Vibration* **3**;10–17. An experimental study of low velocity impacts.
3. J. P. CUSUMANO, M. T. SHARKADY AND B. W. KIMBLE 1994 *Philosophical Transactions of the Royal Society of London A* **347**;421–438. Experimental measurements of dimensionality and spatial coherence in the dynamics of a flexible-beam impact oscillator.
4. S. R. BISHOP, M. G. THOMPSON AND S. FOALE 1996 *Proceedings of the Royal Society of London A* **452**;2579–2592. Prediction of period-1 impacts in a driven beam.
5. Y. CHUMAN, K. MIMURA AND S. TANIMURA 1997 *International Journal of Impact Engineering* **19**;165–174. A sensing block method for measuring impact force generated at a contact part.
6. S. W. SHAW AND P. J. HOLMES 1983 *Journal of Sound and Vibration* **90**;129–155. A periodically forced piecewise linear oscillator.
7. G. S. WHITSON 1987 *Journal of Sound and Vibration* **118**;395–429. Global dynamics of a vibro-impacting linear oscillator.
8. A. B. NORDMARK 1991 *Journal of Sound and Vibration* **145**;275–297. Non-periodic motion caused by grazing incidence in an impact oscillator.
9. S. FOALE AND S. R. BISHOP 1992 *Philosophical Transaction of the Royal Society of London* **338**;547–556. Dynamical complexities of forced impacting systems.
10. C. J. BUDD AND F. DUX 1994 *Nonlinearity* **7**;1191–1124. Intermittency in impact oscillators close to resonance.
11. D. RACICOT AND A. LONGTIN 1995 *Proceedings of the IEEE 17th Annual Conference EMBC and CMBEC*, Vol. 17, 1477–1478, Montréal Canada. Reconstructing dynamics from neural spike trains.
12. K. A. RICHARDSON, T. T. IMHOFF, P. GRIGG AND J. J. COLLINS (1998) *Physical Review Letters* **80**;2485–2488. Encoding chaos in neural spike trains.
13. T. SAUER 1994 *Physical Review Letters* **72**;3811–3814. Reconstruction of dynamical systems from interspike intervals.
14. H. F. POLLARD 1977 *Sound Waves in Solids*. Pion Limited.
15. A. LASOTA AND M. C. MACKAY 1994 *Chaos, Fractals and Noise: Stochastic Aspects of Dynamics*. Berlin: Springer.
16. W. GOLDSMITH 1960 *Impact*. Edward Arnold.
17. F. TAKENS 1981 (D. S. Rand, L. S. Young, editors), *Dynamical Systems and Turbulence*, 366–381, Berlin: Springer. Detecting strange attractors in turbulence.
18. D. S. BROOMHEAD AND G. P. KING 1986 *Physica D* **20**;217–236. Extracting qualitative dynamics from experimental data.
19. T. SAUER 1997 *Journal of Intelligent Systems* **12**;255–265. System identification for chaotic integrate-and-fire dynamics.
20. R. CASTRO AND T. SAUER 1995 *Physical Review E* **55**;287–290. Correlation dimension of attractors through interspike intervals.
21. P. GRASSBERGER AND I. PROCACCIA *Physica D* **9**;189–208. Measuring the strangeness of strange attractors.
22. A. LONTIN AND D. M. RACICOT 1997 (C. D. Cutler and D. T. Kaplan, editors), *Nonlinear Dynamics and Time Series*, 233–239. Providence, RI: American Mathematical Society. Assessment of linear and nonlinear correlations between neural firing events.